J Mol Model (2014) 20:2464
DOI 10.1007/s00894-014-2464-5

ORIGINAL PAPER

Computational study of antimalarial pyrazole alkaloids from *Newbouldia laevis*

Liliana Mammino · Mireille K. Bilonda

Received: 3 March 2014 / Accepted: 7 September 2014 / Published online: 29 October 2014

Abstract Six pyrazole alkaloids of natural origin (isolated from *Newbouldia laevis* in DR Congo) that exhibit antimalarial activity—namely withasomnine, newbouldine, and their *para*-hydroxy and -methoxy derivatives—were investigated theoretically. The nitro derivatives of withasomnine and *para*-hydroxywithasomnine, which show enhanced antimalarial activity, were also studied in this manner. A thorough conformational study was performed in vacuo and in three solvents (chloroform, acetonitrile, and water) at different levels of theory (HF, DFT/B3LYP, and MP2) using different basis sets. Adducts with explicit water molecules were calculated at the HF level. Due to the rigidity of the pyrazole system and the benzene ring, the only factor that influences the energies of withasomnine and newbouldine is the relative orientation of the two ring systems; two orientations are equally preferred. The *para*-hydroxy and -methoxy derivatives show a preference for a planar orientation of the OH and OC bonds. The main stabilizing influence on the nitro derivative of *para*-hydroxywithasomnine is the intramolecular hydrogen bond between the two consecutive functional groups. The calculated adducts show the preferred arrangements of water molecules in the vicinity of the N atoms of the pyrazole system and, for the derivatives, also in the vicinity of the substituents on the benzene ring.

This paper belongs to Topical Collection QUITEL 2013.

Electronic supplementary material The online version of this article (doi:10.1007/s00894-014-2464-5) contains supplementary material, which is available to authorized users.

L. Mammino (✉) · M. K. Bilonda
Department of Chemistry, University of Venda, P/bag X5050, Thohoyandou 0950, South Africa
e-mail: sasdestria@yahoo.com

Keywords Alkaloids · Antimalarials · Natural products · Newbouldine · Pyrazole alkaloids · Withasomnine

Introduction

Malaria is a disease that is responsible for high levels of morbidity and mortality in tropical regions [1]. According to World Health Organization (WHO) reports, it has been estimated that there were nearly 225 million cases of malaria and 781,000 deaths in 2009 [2], 219 million cases and 660,000 deaths in 2010 [3], and 207 million cases and 627,000 deaths in 2012 [4]. 2.23 % of all deaths worldwide are due to malaria. 90 % of all malaria-related deaths occur in sub-Saharan African, where it is one of the main causes of child mortality [3, 4].

Malaria is caused by protozoan parasites of the *Plasmodium* genus that are transmitted to humans via mosquitoes. Among these parasites, *Plasmodium falciparum* is responsible for most of the deaths due to malaria. The greatest challenge in malaria treatment is the fast rate at which *Plasmodium falciparum* develops resistance to drugs—just few years after they enter into clinical use [5, 6]. Thus, the development of new viable drugs must, at the very least, keep the pace with the rate of resistance development in order to avoid the onset of a catastrophic situation. This urgency is also reflected in the appeals from the WHO to expand malaria research.

It is important to understand the molecular origin of the activities of compounds that are already known to have a certain activity – and, therefore, to understand the roles of as many molecular details as possible in the given activity – in order to be able to design related compounds with more potent activity [7]. Computational studies can provide a wealth of information about molecular properties, including descriptors that are relevant to quantitative structure activity relationship (QSAR) studies. Despite this, computational studies of

antimalarials are still not abundant (although they have increased in number in recent years), and they have mostly concerned drugs that are already in clinical use or possible derivatives of them [8–14]. Examples include conformational studies of quinine [15], artemisinin, and related molecules [16], dispiro-1,2,4-trioxolanes [17], and QSAR studies of artemisinin [8, 9], chloroquine and mefloquine [18], and tryptanthrins [19]. Computational studies can also help elucidate the mechanisms of action of known drugs, and this information is important for the design of new drugs. Examples of such studies for antimalarials include the investigation of how artemisinin derivatives disrupt the detoxification of heme by *Plasmodium* [8]; the investigations of the artemisinin pharmacophore and the role of the reductive decomposition of deoxyartemisinins and deoxyartemethers in their antimalarial action [20], the antimalarial activity of dihydroartemisinin derivatives against *P. Falciparum* resistant to mefloquine [21], and the possible roles of interactions between metal cations and antimalarial molecules containing aromatic moieties [22]. Computationally obtainable information has been utilized for the design of new drugs, for instance in the lead optimization for antimalarial acridones [23] or in the design of potent antimalarial bisbenzamidines [24].

Compounds from natural materials utilized in traditional medicine are particularly promising sources of leads for drug development because their ability to exert an activity within a living organism has already been proven. Interest in antimalarial compounds of natural origin is therefore increasing. Many in vitro studies have confirmed the activities of a variety of such materials. Examples include the antiplasmodial activity of extracts from *Esenbeckia febrifuga*, a plant traditionally used to treat malaria in the Brazilian Amazon [25]; the antiplasmodial activity of alkaloids from *Teclea trichocarpa* [26]; the antiplasmodial activity and cytotoxicity of 33 West African plants traditionally used in the treatment of malaria [27], and that of 18 plants used in the traditional medicine of Congo Brazzaville [28]; and the results from the antiprotozoal and cytotoxic screening of the extracts from 45 plants from DR Congo [29].

The work reported in the present paper considered six pyrazole alkaloid compounds with antimalarial activity that were isolated from the root bark of *Newbouldia laevis* (a plant that is endemic to DR Congo and traditionally used in the treatment of malaria, diarrhea, and other diseases [30]), namely: withasomnine (3-phenyl-5,6-dihydro-4*H*-pyrrolo[1,2-b]pyrazole), its *p*-hydroxy and *p*-methoxy derivatives, newbouldine (3-phenyl-3a,5,6-tetrahydro-3*H*-pyrrolo[1,2-b]pyrazole), and its *p*-hydroxy and *p*-methoxy derivatives. These compounds are, respectively, denoted A, B, D, E, F, and G in this work, for the sake of brevity. Their structures are shown in Fig. 1. The half-maximal inhibitory concentration (IC_{50}) value was found to be nearly 122.2 mg/ml for their alcoholic totum. The nitroderivatives of compounds A and B (Fig. 2) were also included in this study, as experiments showed that they possess enhanced antimalarial activity [31, 32]. Withasomnine and its derivatives have no asymmetric centers, whereas newbouldine and its derivatives possess two chiral centers and exhibit optical activity [33].

The antimalarial activity of these compounds is intriguing because such activity is rarely observed in alkaloids containing pyrazole groups, while it appears more frequently in alkaloids containing other groups, such as in quinine, chloroquine, and mefloquine. Thus, the molecular structures of withasomnine and newbouldine are fairly unique among antimalarials, making them suitable candidates for drugs that can overcome *Plasmodium's* drug-resistance. This makes a computational study of these compounds particularly interesting, as it can provide information that may contribute to a better understanding of their activity and to the design of molecules with enhanced activity.

The compounds were studied in vacuo and in three solvents with different polarities, different dielectric constants, and different H-bonding abilities (chloroform, acetonitrile, and water) because their octanol/water partition coefficients suggest that they may be present in non-negligible quantities in media with a broad range of polarities. Adducts with explicit water molecules were also considered because of their significance for solute molecules containing atoms that can form intermolecular hydrogen bonds (H-bonds) with water molecules [34, 35].

The results provide a comprehensive picture of the molecular properties of these compounds, such as conformational preferences in vacuo and in solution, potential energy profiles for the rotation of relevant bonds, harmonic vibrational frequencies, solvent effects, preferred arrangements of explicit water molecules around donor or acceptor sites of the solute molecule, and other features. Tables with detailed results and figures that complement those in the main manuscript are included in the "Electronic supplementary material," ESM.

Computational details

Different calculation methods and different basis sets were utilized to compare their performances and to inform a future study of a high number of antimalarial alkaloids (the information obtained from the results of the different calculation methods for a limited number of compounds aids the selection of the best compromise between result accuracy and computational cost when studying a large number of compounds of the same class).

Calculations in vacuo were performed with full optimization (fully relaxed geometry) at three levels of theory: Hartree Fock (HF) method, Density Functional Theory (DFT) with the B3LYP functional [36–38], and Møller-Plesset Perturbation Theory (MP2). The MP2 results were considered benchmarks

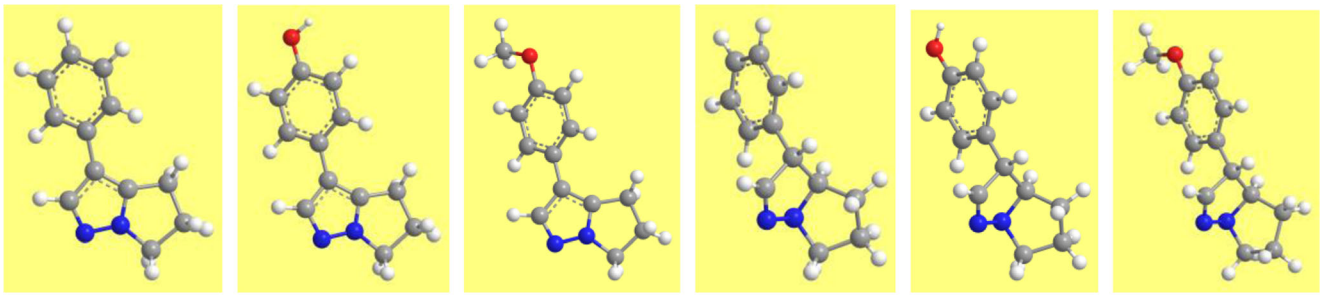

Fig. 1 **A**–**G** The pyrazole alkaloids of natural origin considered in this study, and the letters used to denote them: **A** withasomnine. **B** *p*-hydroxy derivative of withasomnine, **D** *p*-methoxy derivative of withasomnine, **E** newbouldine, **F** *p*-hydroxy derivative of newbouldine, **G** *p*-methoxy derivative of newbouldine

on assessing the performance of the other methods. The following basis sets were utilized in vacuo: 6–31G(d,p), 6–31+G(d,p), 6–31++G(d,p), 6–311G(d,p), 6–311+G(d,p), and 6–311++G(d,p).

Calculations in solution considered three solvents: chloroform, acetonitrile, and water, with dielectric constants of 4.90, 36.64, and 78.39 and estimated (MP2/6–31G(d,p)) dipole moments of 1.4 D, 4.2 D, and 2.2 D, respectively. These solvents cover the ranges of polarity and H-bonding ability of interest for media within a living organism; acetonitrile is also a good model for the medium in membranes. The calculations utilized the polarizable continuum model (PCM, [39, 40]), where the solute is assumed to generate a cavity in the continuum solvent and embed in it. The cavity is modeled through intersecting spheres centered on the nuclei; the intersections are smoothed according to the size of the solvent molecules, which determines the extent to which solvent molecules can come in contact with the solute molecule. The default settings for PCM in the Gaussian 03 package [41] were utilized: IEF (integral equation formalism model, [42–45]) and tesserae average area of 0.200 $Å^2$ for the surface of the cavity around the solute. UAHF radii (united atom topological model applied to radii optimized for the HF/6–31G(d) level) were utilized for the spheres. PCM calculations were performed with re-optimization (fully relaxed geometries) on the geometries optimized in vacuo at the same levels of theory. Only the 6–31G(d,p), 6–31+G(d,p), and 6–31++G(d,p) basis sets were utilized in solution.

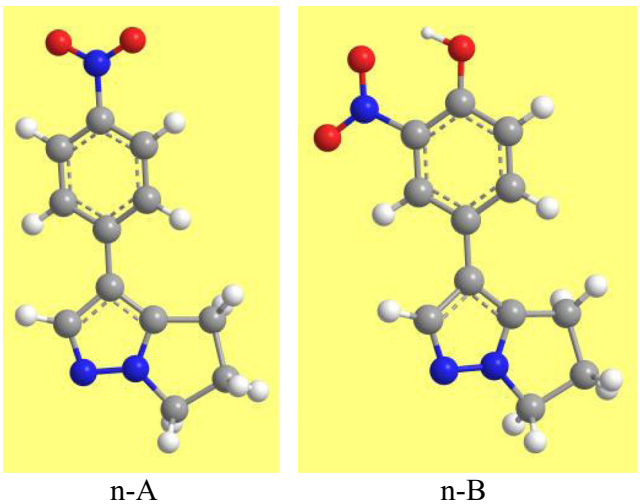

Fig. 2 Nitroderivatives of withasomnine (*left*) and of the *p*-hydroxy derivative of withasomnine (*right*) considered in this study, and the acronyms used to denote them

Harmonic vibrational frequencies were calculated in vacuo and in solution to verify that the optimization results corresponded to true minima.

Adducts with explicit water molecules were calculated for all of the compounds. They were calculated at the HF/6–31G(d,p) level for affordability reasons in view of the large size of the supermolecular structure. The best adducts respond to the approximation of the "first solvation layer" concept utilized in [35], comprising both the water molecules that can H-bond directly to donor or acceptor sites in the solute molecule and those that bridge them and often have a relevant stabilizing effect.

For an adduct containing *n* water molecules, the interaction energy ($\Delta E_{\text{solute-n.aq}}$) between the central molecule and the water molecules H-bonded to it depends on the situation of the given adduct. If the water molecules are not interacting, then

$$\Delta E_{solute-n.aq} = E_{adduct} - E_{solute} - n E_{aq}, \quad (1)$$

where E_{adduct} is the energy of the adduct, E_{solute} is the energy of an isolated solute molecule, and E_{aq} is the energy of an isolated water molecule. If some of the water molecules are H-bonded to each other, then

$$\Delta E_{solute-n.aq} = E_{adduct} - \left(E_{solute} + n E_{aq}\right) - \Delta E_{aq-aq}, \quad (2)$$

where $\Delta E_{\text{aq-aq}}$ is the overall interaction energy between water molecules (largely due to water-to-water H-bonds), and is evaluated by performing a single-point calculation for a group of water molecules identical to that in the adduct, but

without the solute molecule [46]. Both E_{adduct} and $E_{aq\text{-}aq}$ are corrected for BSSE using the counterpoise method [47]. When the geometry of the solute molecule in the adduct does not change significantly from that in the gas phase (as is the case for the compounds considered here), contributions from the deformation energy can be neglected. The same is true for the water molecules.

PCM calculations for adducts optimized in vacuo were performed at the same level, HF/6–31G(d,p), using the single-point option because of the excessive computional costs of PCM re-optimization of the bulky supermolecular structures of the adducts.

Natural bond orbital [48–51] analysis was utilized to get detailed information about the charges on the more electronegative atoms (N and O) in different media and also in the adducts with explicit water molecules.

For the sake of brevity, acronyms for the media are utilized in the text when reporting values (*vac* for vacuum, *chlrf* for chloroform, *actn* for acetonitrile, and *aq* for water).

All of the energy values reported in the text are expressed in kcal/mol, and all of the distances are in Å.

Results

Results in vacuo

The same atom numbering was utilized for corresponding positions in all of the molecules considered in order to facilitate comparisons of geometric features. Although this implies that some atom numbers may have been be skipped in some structures, it is considered that the potential for quick comparisons is more important. Figure 3 shows the atom numbering schemes for three representative cases, and the caption explains the changes for the other molecules.

For each compound, conformers are denoted by adding a number after the letter or acronym denoting the compound, and this number increases as the relative energy of the conformer increases. When no number is present, the lowest-energy conformer is being referred to. This is acceptable in most analyses because the energy difference between conformers is small and they show similar behavior, with the exception of the conformers of compound n-B.

The rigidity of the two ring systems (benzene and pyrazole) means that the mutual orientation of these systems is the only factor that can distinguish conformers of compounds A and E. A flexible scan of the rotation of the C–C bond between the two ring systems was carried out for A and E at different levels of theory (HF/6–31G (d,p), DFT/6–31G(d,p), and MP2/6–31G(d,p)). The resulting potential energy profiles are shown in Fig. 4. These results, as well as separate calculations performed with fully relaxed geometries around the identified minima, show that the energies of the conformers corresponding to minima with different mutual orientations of the ring systems differ by less than 0.3 kcal/mol, with all the calculation methods used (e.g., they differ by 0.232 kcal/mol in the HF results, 0.284 kcal/mol in the DFT results, and 0.198 kcal/mol in the MP2 results for A).

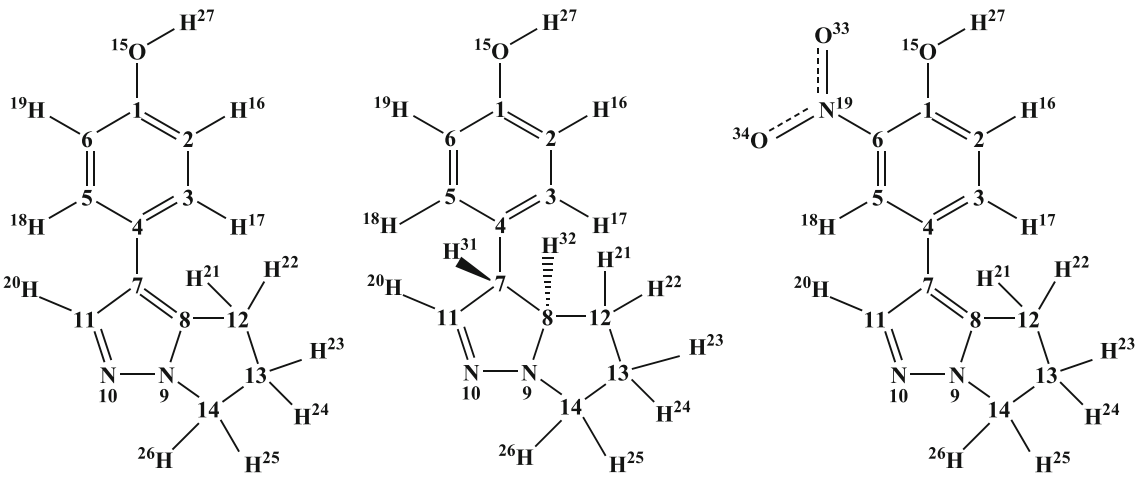

Fig. 3 Schemes of the atom numbering utilized for the compounds considered in this work. The carbon atoms are represented only by their numbers; the symbols of all the other atoms are shown explicitly. The same atom numbering is utilized for atoms in corresponding positions in all of the compounds investigated here, in order to facilitate comparisons. Compounds B, F, and n-B are shown as examples. In compounds A and E, the number 15 is assigned to the H atom attached to C1; in compounds D, F, G, and H, it is assigned to the O atom attached to C1. The C atom of the methoxy group in D and G is given the number 27, and the H atoms attached to it are given the numbers 28, 29, and 30. Because of this, the additional H atoms attached to C7 and C8 in E, F, and G are given the numbers 31 and 32, respectively. The N of the nitro group attached to C1 in n-A is given the number 15 and the N of the nitro group attached to C6 in n-B is given the number 19; the two O atoms of these nitro groups are numbered 33 and 34

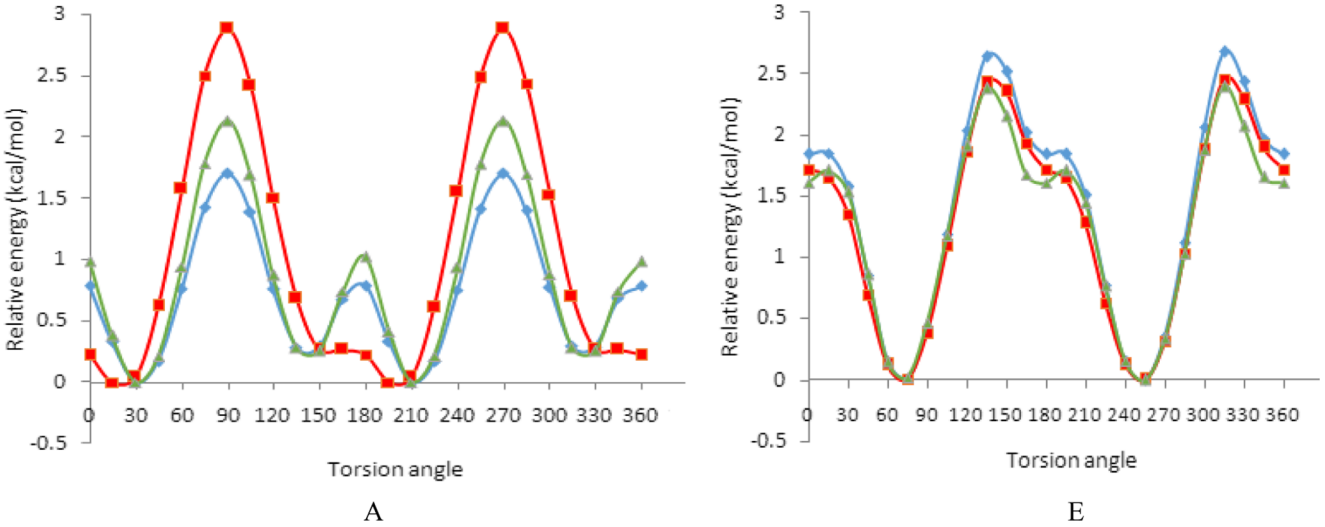

Fig. 4 Potential energy profiles for the flexible scan of the C11–C7–C4–C5 torsion angle (rotation of the C7–C4 bond between the two ring systems) in compounds A (*left*) and E (*right*). HF/6–31G(d,p) (*diamonds*), DFT/B3LYP/6–31G(d,p) (*squares*), and MP2/6–31G(d,p) (*triangles*) results in vacuo are plotted

For the *p*-hydroxy derivatives, an additional geometry difference arises from the orientation of the OH group. A flexible scan of the rotation of the C1–O15 bond (Fig. 5) shows a prefe geometry rence for OH to be coplanar with the ring—consistent with what is observed for phenols in general [52, 53]. Comparison with a similar scan for phenol (Fig. 6) shows that the barrier heights are almost the same. As long as the OH is planar, its orientation to one or another side does not imply significant energy differences in compounds B and F. The difference between the two orientations is less than 0.1 kcal/mol, which indicates that the presence of the pyrazole ring does not influence the orientation preferences of the phenol OH.

Similarly, for compounds D and G, an additional geometry difference arises from the orientation of the OCH_3 group. This group prefers to be oriented with the C atom coplanar with the benzene ring—consistent with what is observed for an OCH_3 group attached to a benzene ring when there is no steric hindrance from neighboring groups [54].

For the nitroderivative n-A, an additional geometric feature arises from the orientation of the NO_2 group. A flexible scan of the rotation of the C1–N15 bond (Fig. 7) shows that a planar orientation of the whole NO_2 group is preferred. This is consistent with what is reported for nitrobenzenes [55–57]. A similar scan for nitrobenzene (Fig. 7) shows that the minima coincide and the maxima nearly coincide in the MP2 results (difference of 0.27 kcal/mol), whereas they differ slightly with the other methods used here (by 0.78 kcal/mol with HF; by 0.98 kcal/mol with DFT). Overall, these results confirm that

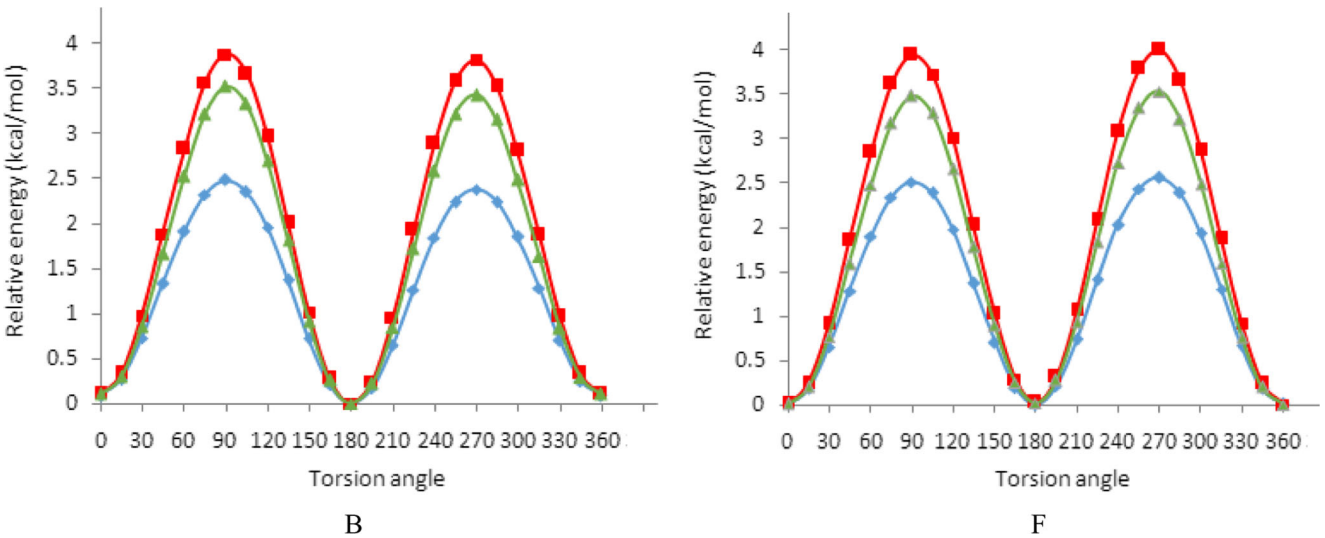

Fig. 5 Potential energy profiles for the flexible scan of the C2–C1–O15–H27 torsion angle (rotation of the C1–O15 bond) in compounds B (*left*) and F (*right*). HF/6–31G(d,p) (*diamonds*), DFT/B3LYP/6-31G(d,p) (*squares*), and MP2/6–31G(d,p) (*triangles*) results in vacuo are plotted

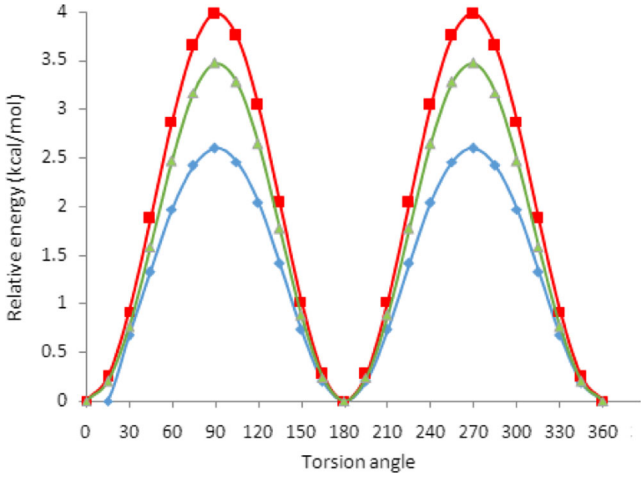

Fig. 6 Potential energy profiles for the flexible scan of the rotation of the C–O bond in phenol. HF/6–31G (d,p) (*diamonds*), DFT/B3LYP/6–31G(d,p) (*squares*), and MP2/6–31G(d,p) (*triangles*) results in vacuo are plotted. Although a 180° rotation would be sufficient in this case due to the symmetry of the molecule, a 360° rotation was carried out to facilitate comparisons with the scans of B and F

the pyrazole system exerts a negligible influence on the geometry preferences of a *para* substituent in the benzene ring.

For nitroderivative n-B, an important geometry difference arises from the possibility of the presence or absence of an intramolecular hydrogen bond (IHB) between the OH group and one of the O atoms of the NO_2 group. Table 1 shows the relative energy of the higher energy conformer (the one without the IHB) with respect to the lowest energy conformer (whose relative energy is taken as zero) in the results of the calculation methods utilized and for all the media considered. Figure 8 shows a flexible scan of the rotation of the OH group. The scan shows similarities with that of the rotation of the phenol OH engaged in the IHB with the sp^2 O of the acyl group in acylphloroglucinols [58]. In both cases, the scan starts from a conformer in which the IHB is present, and the rotation of the phenol OH gradually removes the IHB. The acceptor O atom also rotates, "following" the H atom until the interaction between the two vanishes completely. In this way, the acceptor O shifts out of plane and remains out of plane in the conformer without the IHB, thus partially smoothing the repulsion between the two O atoms. The height of the barrier to the removal of an IHB by 180° rotation of the donor gives an indication of the strength of the IHB [59]. In the case of n-B, the barrier height is close to 11 kcal/mol in the HF and MP2 results, and is close to 15 kcal/mol in the DFT results.

The energy values reported in Table 1 correspond to the increase in energy upon the removal of the IHB ($\Delta E_{\text{IHB-removal}}$). Although these values are larger than the IHB actual energy because they include the contribution of the O↔O repulsion [58, 60], the fact that the repulsion is smoothed by the off-plane shift of the acceptor O reduces the overestimation. The DFT results tend to overestimate the energies of H-bonds, so the HF and MP2 results provide more realistic evaluations of their strength and of the relative energy of the conformer from which the IHB is removed.

The geometric parameters of the molecules considered differ only slightly in the results of the different methods utilized. The length of the C4–C7 bond between the benzene ring and the pyrazole system is ~1.47 Å for A, B, and D and 1.51 Å for E, F, and G with all methods, and the N9–N10 bond is ~1.34 Å for A, B, and D and ~1.40 Å for E, F, and G.

Results in solution

The solvent effect (free energy of solvation, ΔG_{solv}) is negative for all these compounds and in all of the solvents

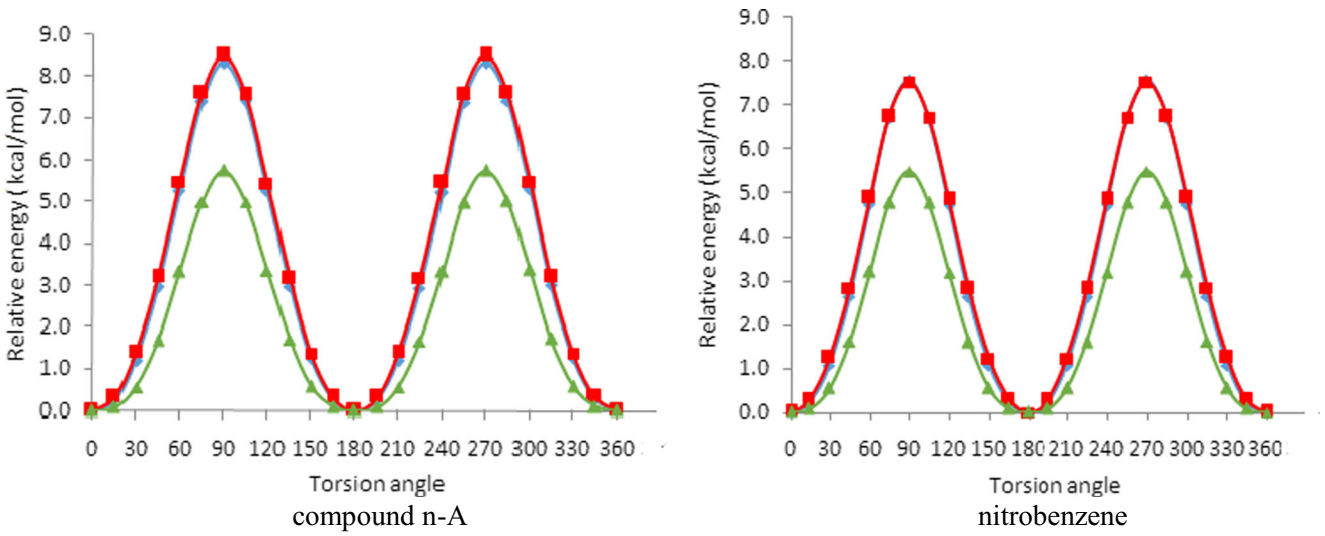

Fig. 7 Potential energy profiles for the flexible scan of the rotation of the C–N bond in compound n-A (rotation of the C2–C1–N15–O33 torsion angle) and in nitrobenzene. HF/6–31G(d,p) (*diamonds*), DFT/B3LYP/6–31G(d,p) (*squares*) and MP2/6–31G(d,p) (*triangles*) results in vacuo are plotted

Table 1 Relative energy of the higher energy conformer of compound n-B (conformer n-B-2), corresponding to the lowest energy orientation of the ring systems, and differing from the lowest energy conformer (n-B-1, relative energy 0.000 kcal/mol) by the absence of the intramolecular hydrogen bond between the OH group and the NO_2 group. Results obtained from different calculation methods, in vacuo and in the three solvents considered, are shown

Calculation method	Relative energy (kcal/mol)			
	In vacuo	In chloroform	In acetonitrile	In water
HF/6–31G(d,p)	9.857	6.511	5.156	2.350
MP2/6–31G(d,p)	9.355	6.479	5.277	2.457
DFT/B3LYP/6–31G(d,p)	11.783	9.012	7.734	4.801
HF/6–31+G(d,p)	9.435	6.045	4.668	1.847
MP2/6–31+G(d,p)	7.782	4.751	2.880	0.565
DFT/B3LYP/6–31+G(d,p)	11.190	7.976	6.593	3.556
HF/6–31++G(d,p)	9.453	6.063	4.686	1.866
MP2/6–31++G(d,p)	7.829	5.618	3.518	0.612
DFT/B3LYP/6–31++G(d,p)	11.230	8.049	6.665	3.602

considered. The magnitude of ΔG_{solv} is smaller for acetonitrile, greater for chloroform, and greatest for water. It is considerably larger for B than for A and D, and for F than for E and G, which is consistent with the effect of the presence of a phenol OH in B and F, enabling stronger solute–solvent interactions (H-bonds). It does not differ significantly between A and D or between E and G, consistent with the weaker effect of an OCH_3 group on solute–solvent interactions. It is about 1 kcal/mol smaller for E, F, and G than for A, B, and D, respectively, suggesting that the pyrazole system in withasomnine and its derivatives interacts more favorably with the solvent than the pyrazole system in newbouldine and its derivatives. The trends for ΔG_{solv} and its electrostatic component G_{el} are similar in the results of all the calculation methods utilized. The addition of diffuse functions on the heavy atoms increases the magnitude of ΔG_{solv} somewhat, whereas the further addition of diffuse functions on the H atoms does not bring significant changes.

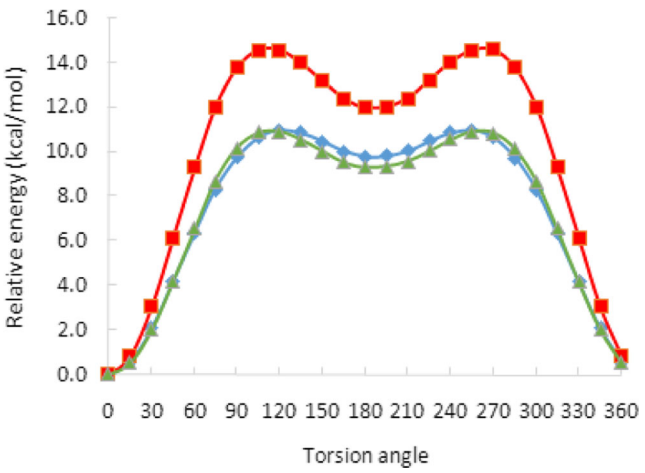

Fig. 8 Potential energy profiles for the flexible scan of the C6–C1–O15–H27 torsion angle (rotation of the OH group) in compound n-B. HF/6–31G(d,p) (*diamonds*), DFT/B3LYP/6–31G(d,p) (*squares*), and MP2/6–31G(d,p) (*triangles*) results in vacuo are plotted

The geometric features of the molecules are very similar for all the media considered, as are the energy differences between conformers, except in the case of n-B, where the gap between the conformers with and without the IHB between the OH and the NO_2 groups decreases sharply as the solvent dielectric constant increases (Table 1).

The potential energy profiles for the rotation of the relevant bonds considered in vacuo were also calculated in solution, mostly at the HF/6–31G(d,p) level. The height of the barrier to the rotation of the bond between the two ring systems (C4–C7) in A increases as the solvent dielectric constant increases, and it is≈0.9 kcal/mol higher in water than in vacuo. The barrier to the rotation of the C1–O15 bond in B also increases with increasing solvent ε, but less markedly than for C4–C7. The barrier to the rotation of the O15–C27 bond in D and G is very similar in all of the media, with a slight decrease noted in water for G. The barrier to the rotation of the C1–N15 bond in n-A is also very similar in all of the media, with a slight decrease noted as the solvent ε increases. The barrier to the rotation of the OH group in n-B decreases sharply as the solvent ε increases, and the calculated value in water is less than half the value obtained in vacuo.

n-B poses the challenging question of the fate of the IHB in solution: is it maintained, substantially weakened or broken? The energy gap between the conformers with and without the IHB decreases sharply as the solvent ε increases, and so does the energy barrier to the removal of the IHB by rotating the donor by 180°. However, an estimation of the IHB strength in solution cannot be linked to the energy difference between the two conformers, because the stabilization by the solvent is greater for the conformer without the IHB than for the conformer with the IHB [61]. This effect is different for different solvents and increases with increasing solvent ε; it is considerably higher for solvents that are capable of forming intermolecular H-bonds with the solute molecule, as the removal of an IHB leaves its donor and acceptor atoms available to form H-bonds with the solvent molecules. The situation is

Table 2 Parameters of the intramolecular hydrogen bond (IHB) of compound n-B according to the results of different calculation methods obtained in different media. The calculation methods used are denoted by the following acronyms: HF for HF/6–31G(d,p), HF+for HF/6–31+G(d,p), HF++ for HF/6–31++G(d,p), DF for DFT/6–31G(d,p), DF+for DFT/6–31+G(d,p), DF++ for DFT/6–31++G(d,p), MP for MP2/6–31G(d,p), MP+for MP2/6–31+G(d,p), MP++ for MP2/6–31++G(d,p)

Method	O···H bond length (Å)				O···O distance (Å)				OĤO bond angle			
	vac	chlrf	actn	aq	vac	chlrf	actn	aq	vac	chlrf	actn	aq
HF	1.825	1.833	1.838	1.862	2.601	2.606	2.608	2.618	137.0	136.5	136.3	134.6
HF+	1.833	1.843	1.848	1.875	2.604	2.608	2.611	2.622	136.3	135.7	135.5	133.6
HF++	1.833	1.842	1.847	1.876	2.604	2.609	2.611	2.623	136.3	135.8	135.5	133.6
DFT	1.689	1.693	1.695	1.716	2.561	2.563	2.564	2.574	144.9	144.7	144.6	143.2
DFT+	1.707	1.712	1.714	1.740	2.567	2.570	2.570	2.582	143.4	143.1	142.9	141.1
DFT++	1.688	1.712	1.713	1.740	2.561	2.569	2.569	2.582	145.0	143.1	143.0	141.2
MP	1.747	1.751	1.754	1.773	2.599	2.601	2.603	2.611	143.5	143.2	143.0	141.6
MP+	1.747	1.751	1.755	1.773	2.599	2.601	2.603	2.611	143.5	143.2	143.0	141.6
MP++	1.747	1.751	1.754	1.773	2.599	2.601	2.603	2.611	143.5	143.2	143.0	141.6

analogous to that discussed in [60] for the IHB between a phenol OH and an sp^2 O bonded to a C atom *ortho* to the OH on the benzene ring. The energy difference between the two conformers (the conformer with the IHB and the conformer without the IHB) is not solely determined by intramolecular factors (IHB removal, geometry changes caused by the removal, O↔O repulsion) but also by an "external" factor, the solvent stabilization, and this factor is greater for the conformer without the IHB. This would suggest that the strength of the IHB is greater than the energy difference between the two conformers.

The polarization of the electron cloud due to the solvent field and depending on the solvent ε, tends to weaken the strength of the IHB. On the other hand, local geometry factors in the solute molecule may play significant roles. Thus, it is not easy to find criteria that lead to a reasonable approximation for the strength of the IHB in solution. The lack of relevant experimental techniques [62] implies an absence of experimental values that could provide reliable references for the assessment of theoretical results. Features that are influenced by the solvent effect (including the height of the rotational barrier to the removal of the IHB through 180° rotation of the donor, or the redshift of the OH vibrational frequency) do not represent reliable references because of the same reason—the different solvent effect on the two conformers (i.e., the conformer with the IHB and the conformer without the IHB). A factor intrinsic to the IHB—such as its length (Table 2)—can be more reliably linked to the IHB strength, with shorter lengths corresponding to stronger IHBs. However, local geometric features can considerably influence the possibility of variations in the IHB length. In the case of n-B, the possibility that the IHB length varies is considerably restricted by the rigidity of the benzene ring. However, this factor also favors the permanence of the IHB in solution without any dramatic decrease in strength, because the rigidity of the benzene ring does not favor the types of geometry changes that could break the IHB. In this regard, this case is analogous to other cases in which an IHB forms between groups at consecutive positions on a benzene ring (e.g., in hydroxybenzenes [62, 63] and acylphloroglucinols [60]).

The presence of an H-bond causes a decrease in the IR frequencies of the donor OH. The phenomenon is called redshift. The redshift is greater for stronger H-bonds [64]. However, the value of the redshift can only be viewed as an indication of the IHB strength in vacuo, as the solvent effect may introduce additional factors in solution. The redshift is calculated as the difference from the frequency of a conveniently selected free OH (an OH that is not engaged in an IHB). In the case of n-B-1 (the conformer of n-B with the IHB), the most apt reference appears to be the frequency of the OH in compound B; however, the frequency of the conformer without the IHB (n-B-2) was also utilized as a separate reference to obtain a complementary set of information. The values are somewhat smaller in the latter case. The redshift values for n-B-1 are considerably different in the results of the calculation methods utilised (despite the frequency values being scaled according to the method). For instance, the values (cm^{-1}) in vacuo range from 128.7 (HF) to 243.3 (MP2) to 401.0 (DFT); the last value is consistent with the known tendency of DFT to overestimate H-bond strengths.

The dipole moments of these compounds increase steadily as the solvent ε increases, because of the greater polarization of the solute charges by solvents with greater ε. For instance, in the MP2/6–31++G(d,p) results, the dipole moment (in debye) ranges from 3.4 (vac) to 4.8 (aq) for A-1, from 4.4 (vac) to 6.5 (aq) for B-1, from 2.5 (vac) to 3.5 (aq) for D-1, from 2.6 (vac) to 3.7 (aq) for E-1, from 3.2 (vac) to 4.86 (aq) for F-1, from 2.7 (vac) to 3.6 (aq) for G-1, from 7.3 (vac) to 9.0 (aq) for n-A-1, from 7.2 (vac) to 9.4 (aq) for n-B-1, and from 9.5 (vac) to 12.7 (aq) for n-B-2.

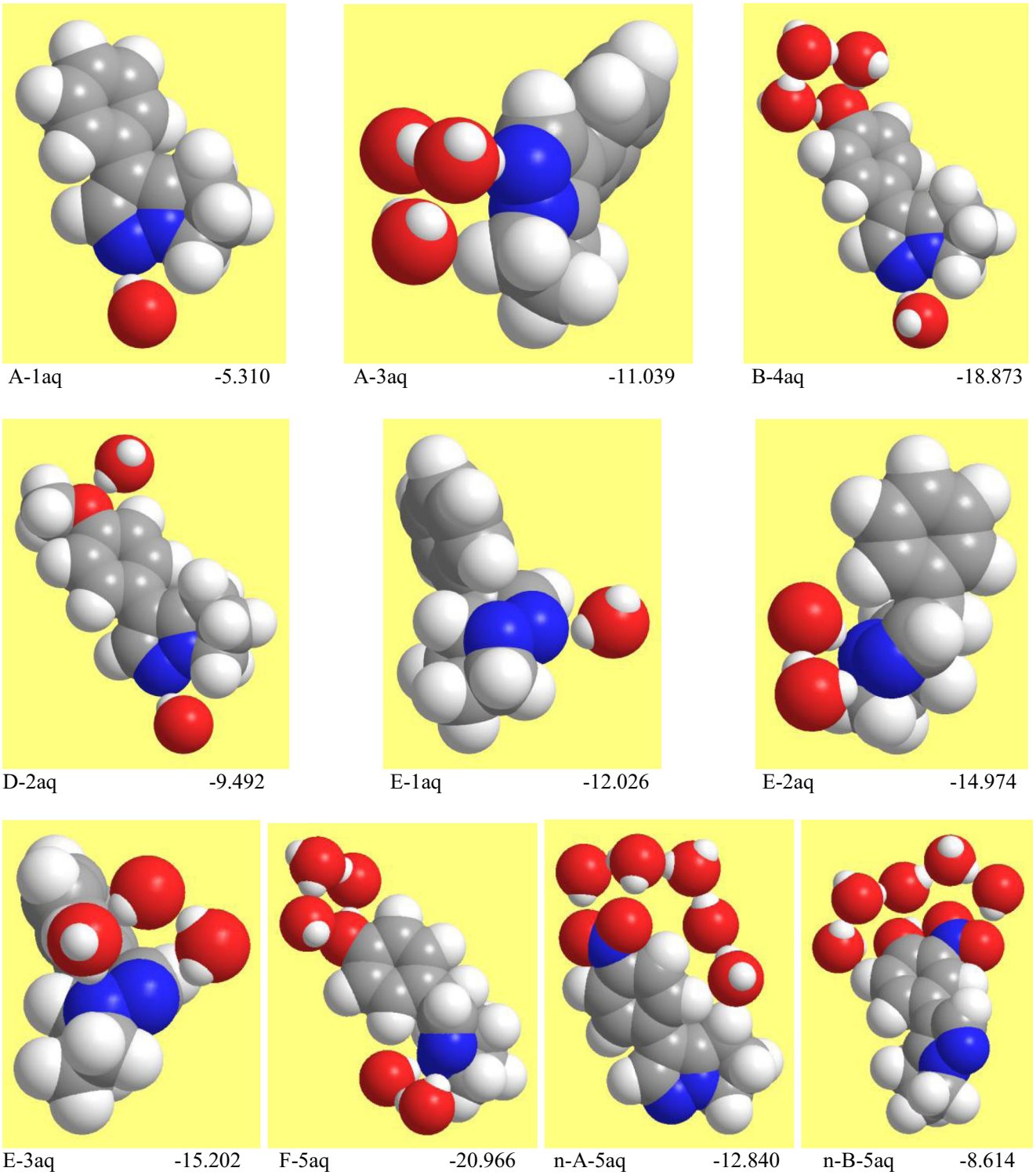

Fig. 9 Selected adducts of the calculated compounds with explicit water molecules. The molecule–water interaction energy (kcal/mol, corrected for BSSE) is reported under each image

Values for the HOMO–LUMO energy gap are similar in magnitude in the HF and MP2 results, whereas the values obtained from DFT calculations are much smaller. This is a known phenomenon associated with DFT [65]; however, although individual values may be unrealistic, trend identification on the basis of those values is reasonable. For instance, the gap (in kcal/mol) for structure A in vacuo is 208.2 (HF/6–31++G(d,p)), 208.7 (MP2/6–31++G(d,p)), and 121.0 (DFT/B3LYP/6–31++G(d,p)). The values do not differ considerably in the media considered; when diffuse functions

are present, the values show a tendency to slightly increase as the solvent ε increases.

Adducts with explicit water molecules

Adducts with explicit water molecules were calculated for all of the compounds considered. In A and E, there is only one region capable of H-bonding with water molecules—the two N atoms in the pyrazole system. The other compounds have a second region around the groups attached to the benzene ring (OH or OCH_3 groups and, for the nitroderivatives, also NO_2). The two regions are sufficiently distant to be completely independent in the ways in which they H-bond with water molecules, as H-bonds between the water molecules attached to the N atoms and the water molecules attached to the group on the benzene ring are not possible.

Different numbers and arrangements of water molecules in the two regions were considered. Figure 9 shows most of the calculated adducts and their water–molecule interaction energies. For the pyrazole region, the best arrangement comprises three water molecules—two attached to the two N atoms and a third water molecule bridging them. This agrees with the results from a computational and experimental study of the hydration of pyrazole [66], which found that the pyrazole–$(H_2O)_3$ adduct has the best water–pyrazole interaction energy. For the region around the OH group in B and F, the best arrangement is consistent with the known tendency to have a square of O atoms around the OH of a phenol [67] or alcohol [68].

For all of the adducts, the geometry of the central molecule remains practically undisturbed. For compound n-B, the length of the IHB increases somewhat in the adducts and the bond angle decreases. The adduct geometries show the simultaneous presence of the IHB and H-bonds with water molecules—a phenomenon observed for several molecules with groups attached at consecutive positions on a benzene ring that are capable of forming H-bonds (e.g., hydroxybenzenes with consecutive OH groups [63, 69–71]). While PCM optimization rarely leads to IHB breaking (because PCM does not take solute–solvent H-bonds into account explicitly [61]), adduct optimization may lead to IHB breaking [72] and the formation of H-bonds with water molecules. Therefore, the simultaneous presence of the IHB and H-bonds with water molecules in the calculated adducts (with geometry adjustments to accommodate this simultaneous presence) supports the hypothesis that the IHB in n-B-1 is maintained in solution, including in water solution.

The adducts were also considered as solutes in single-point PCM calculations in water, which were performed at the same HF/6–31G(d,p) level at which the adducts were calculated. The magnitude of ΔG_{solv} decreases as the number of water molecules in the adduct increases. This is consistent with the fact that the water molecules closest to the solute molecule are incorporated into the adduct, so their interactions with the central molecule (which represent the most important contribution to the solute–solvent interaction) are no longer part of the bulk solvent effect. The magnitude of the electrostatic contribution to ΔG_{solv} (G_{el}) increases as the number of water molecules in the adduct increases.

Discussion and conclusions

This computational study of eight pyrazole alkaloids has identified conformational preferences, factors influencing conformer stability, solvent effects for solvents that mimic the range of media in which a drug molecule may exert its action within a living organism, and other molecular properties, such as dipole moments, frontier orbital energy gaps, vibrational frequencies (harmonic approximation), properties of the IHB for compound n-B, and preferential arrangements of water molecules in the vicinity of the sites that are capable of forming H-bonds with water molecules. These results can be used as a starting point for other computational studies, such as an investigation of possible reaction pathways. In turn, such an investigation could lead to a better understanding of the mechanisms of the biological activity of the compounds. The comparison of the performance of the different calculation methods used in this work is relevant to the selection of cost-convenient and sufficiently informative computational methods for an envisaged study of a high number of other alkaloids with antimalarial activity. This envisaged study — which will be the object of a separate work — is expected to provide sufficient information to enable realistic attempts to relate the antimalarial activity to the molecular properties of active alkaloids.

References

1. Snow RW, Guerra CA, Noor AM, Myint HY, Hay SI (2005) Nature 434(7030):214–217
2. World Health Organization (2010) World malaria report 2010 summary. http://www.who.int/malaria/world_malaria_report_2010/malaria2010_summary_keypoints_fr.pdf
3. World Health Organization (2011) World malaria report 2011 summary. http://www.who.int/malaria/world_malaria_report_2011/wmr2011_summary_keypoints_fr.pdf
4. World Health Organization (2012) World malaria report 2012 summary. http://www.who.int/malaria/publications/world_malaria_report_2012/report/en/
5. Mital A (2007) Curr Med Chem 14:759–773
6. Marco M, Cateron MT (2012) Curr Top Med Chem 12:408–444
7. Alagona G, Ghio C (2009) Phys Chem Chem Phys 11:776–790
8. Pinheiro JC, Kiralj R, Ferreira MMC, Romero OAS (2003) QSAR Comb Sci 22:830–842
9. Avery MA, Gao F, Chong WKM, Methrotra S, Millhous WK (1993) J Med Chem 36:4264–4275

10. Avery MA, Methrotra S, Johnson TL, Brak JD, Vroman JA, Miller R (1996) J Med Chem 39:4149–4155
11. O' Neill PM, Willock DJ, Hawley SR, Bray PG, Storr RC, Ward SA, Park BK (1997) J Med Chem 40:437–348
12. De DYD, Krogstad FM, Byers LD (1998) J Med Chem 41:4918–4926
13. O' Neill PM, Searle NL, Kan KW, Storr RC, Maggs JL, Ward SA, Raynes K, Park BK (1999) J Med Chem 42:5487–5493
14. Cardoso FJB, Da Costa RB, De Figueiredo AF, Barbosa JP, Nava I Jr, Pinheiro JC, Romero OAS (2007) Internet Electron J Mol Des 6: 122–134
15. Silva THA, Oliviera AB, De Almeida WB (1997) Struct Chem 8(2): 1–13
16. Galasso V, Kovač B, Modelli A (2007) Chem Phys 335:141–154
17. Moroni L, Salvi PR (2006) Chem Phys Lett 419:75–80
18. Bhattacharjee AK, Kyle DE, Vennerstrom JL, Milhous WK (2002) J Chem Inf Comput Sci 42:1212–1220
19. Bhattacharjee AK, Hartell MG, Nichols, Hicks RP, Stanton B, van Hamont JE, Milhous WK (2004) Eur J Med Chem 39:59–67
20. Drew MGB, Metcalfe J, Dascombe MJ, Ismail FMD (2007) J Mol Struct (THEOCHEM) 823:34–46
21. Pinheiro JC, Ferreira MMC, Romero OAS (2001) J Mol Struct (THEOCHEM) 572:35–44
22. Bhattacharjee AK (2000) J Mol Struct (THEOCHEM) 529:193–201
23. Winter RW, Kelly JX, Smilkstein MJ, Dodean R, Bagby GC, Rathbun RK, Levin JI, Hinrichs D, Michael MK (2006) Exp Parasitol 114:47–56
24. Cruz-Monteagudo M, Borges F, Perez González M, Dias Soeiro Cordeiro NM (2007) Bioorg Med Chem 15:5322–5339
25. Dolabela MF, Oliveira SG, Nascimento JM, Peresjm, Wagner H, Povoa MM, Oliveira AB (2008) Phytomedicine 15:367–372
26. Muriithi MW, Abraham WR, Addae-Kyereme J, Scowen I, Croft SL, Gitu PM, Kendrick H, Njagi ENM, Wright CW (2002) J Nat Prod 65: 956–959
27. Zirihi N, Mambu L, Guédé-Guina F, Bodo B, Grellier P (2005) J Ethnopharmacol 98:281–285
28. Mbatchi SF, Mbatchi B, Banzouzi JT, Bansimba T, Nsonde Ntandou GF, Ouamba JM, Berry A, Benoit-Vical F (2006) J Ethnopharmacol 104:168–174
29. Mesia GK, Tona GL, Nanga TH, Cimanga RK, Apers S, Cos P, Maes L, Pieters L, Vlietinck AJ (2008) J Ethnopharmacol 115:409–415
30. Mifundu N (2011) Etude in vitro de l'activité antipaludique des alcaloïdes de *Newboldia laevis*. Thesis. University of Kinshasa, Kinshasa
31. Mudimba M (2014) Activité antipaludique des alcaloïdes nitré de *Newboldia laevis*. Thesis. University of Kinshasa, Kinshasa
32. Bosange L (2008) Evaluation in vitro de l'activité antipaludique des alcaloïdes nitré de *Newboldia laevis*. Thesis. University of Kinshasa, Kinshasa
33. Adesanya SA, Nia R, Fontaine C, Pays M (1994) Phytochemistry 35(4):1053–1055
34. Mammino L, Kabanda MM (2011) Comparison of possible conformations and conformational preferences of the Z and E isomers of caespitate. In: Recent Researches in Chemistry, Biology, Environment and Culture (Proc COMPUCHEM '11/BIO '11/EED '11/ICBB '11/ICAC '11), Montreux, Switzerland, 29–31 Dec 2011, pp 119–124
35. Mammino L, Kabanda MM (2010) Int J Quantum Chem 110(13): 2378–2390
36. Becke AD (1992) J Chem Phys 96:9489
37. Becke AD (1993) J Chem Phys 98:5648–5652
38. Lee C, Yang W, Parr RG (1998) Phys Rev B 37:785–789
39. Tomasi J, Persico M (1994) Chem Rev 94:2027–2094
40. Tomasi J, Mennucci B, Cammi R (2005) Chem Rev 105:2999–3093
41. Frisch MJ, Trucks GW, Schlegel HB, Scuseria GE, Robb MA, Cheeseman JR, Montgomery JA, Vreven T, Kudin KN, Burant JC, Millam JM, Iyengar SS, Tomasi J, Barone V, Mennucci B, Cossi M, Scalmani G, Rega N, Petersson GA, Nakatsuji H, Hada M, Ehara M, Toyota K, Fukuda R, Hasegawa J, Ishida M, Nakajima T, Honda Y, Kitao O, Nakai H, Klene M, Li X, Knox JE, Hratchian HP, Cross JB, Adamo C, Jaramillo J, Gomperts R, Stratmann RE, Yazyev O, Austin AJ, Cammi R, Pomelli C, Ochterski JW, Ayala PY, Morokuma K, Voth GA, Salvador P, Dannenberg JJ, Zakrzewski VG, Dapprich S, Daniels AD, Strain MC, Farkas O, Malick DK, Rabuck AD, Raghavachari K, Foresman JB, Ortiz JV, Cui Q, Baboul AG, Clifford S, Cioslowski J, Stefanov BB, Liu G, Liashenko A, Piskorz P, Komaromi I, Martin RL, Fox DJ, Keith T, Al-Laham MA, Peng CY, Nanayakkara A, Challacombe M, Gill PMW, Johnson B, Chen W, Wong MW, Gonzalez C, Pople JA (2003) Gaussian 03, version D 01. Gaussian, Inc., Pittsburgh
42. Mennucci B, Tomasi J (1997) J Chem Phys 106:5151–5158
43. Mennucci B, Cancès E, Tomasi J (1997) J Phys Chem B 101:10506–10517
44. Cancès E, Mennucci B, Tomasi J (1997) J Chem Phys 107:3032–3041
45. Barone V, Cossi M, Tomasi J (1998) J Comput Chem 19:404–417
46. Alagona G, Ghio C (2006) J Phys Chem A 110:647–659
47. Boys SF, Bernardi F (1970) Mol Phys 19:553
48. Reed AE, Weinhold F (1983) J Chem Phys 78(6):4066–4074
49. Reed AE, Weinhold F (1985) J Chem Phys 83(4):1736–1741
50. Reed AE, Weinstock RB, Weinhold F (1985) J Chem Phys 83(2): 735–747
51. Carpenter JE, Weinhold F (1988) J Mol Struct THEOCHEM 169:41–62
52. Spoliti M, Bencivenni L, Quirante JJ, Ramondo F (1997) J Mol Struct THEOCHEM 390:139–148
53. Rudyk R, Molina MAA, Yurquina A, Gómez MI, Blanco SE, Ferretti FH (2004) J Mol Struct THEOCHEM 673:231–238
54. Kabanda MM, Mammino L (2012) Int J Quantum Chem 112:3691–3702
55. Irle S, Krygowski JTM, Niu JE, Schwarz WHE (1996) J Org Chem 60:6744–6755
56. Politzer P, Lane P, Jayasuriya K, Domelsrnith LN (1987) J Am Chem Soc 109:1899–1901
57. Staikova M, Csizmadia IG (1999) J Mol Struct THEOCHEM 467: 181–186
58. Mammino L, Kabanda MM (2009) J Mol Struct THEOCHEM 901: 210–219
59. Buemi G, Zuccarello F (2002) J Mol Struct THEOCHEM 581: 71–85
60. Mammino L, Kabanda MM (2009) J Phys Chem A 113(52):15064–15077
61. Alagona G, Ghio C (2002) Int J Quantum Chem 90:641–656
62. Korth HG, de Herr MJ, Mulder P (2002) J Phys Chem A 106:8779
63. Mammino L, Kabanda MM (2011) Int J Quantum Chem 111:3701–3716
64. Gilli G, Gilli P (2000) J Mol Struct 552:1–15
65. Turner A (2008) How to analyse the orbitals from a Gaussian calculation. https://www.wiki.ed.ac.uk/display/EaStCHEMresearchwiki/How+to+analyse+the+orbitals+from+a+Gaussian+calculation
66. Ramondo F, Tanzi L, Campetella M, Gontrani L, Mancini G, Pieretti A, Sadun C (2009) Phys Chem Chem Phys 11:9431–9439
67. Ahn DS, Jeon IS, Jang SH, Park SW, Lee S, Cheong W (2003) Bull Korean Chem Soc 24:695–702
68. Mammino L (2009) Chem Phys Lett 473:354–357
69. de Heer MJ, Korth HG, Mulder P (1999) J Org Chem 64:6969–6975
70. de Heer MI, Mulder P, Korth HG, Ingold KU, Lusztyk J (2000) J Am Chem Soc 122:2355–2360
71. Cappelli C, Mennucci B, Monti S (2005) J Phys Chem A 109:1933–1943
72. Mammino L, Kabanda MM (2008) Int J Quantum Chem 108:1772–1791